





In-Situ Calibration Method of Online Junction Temperature Estimation in IGBTs for Electric Vehicle Drives

Wei Lai , Member, IEEE, Yunhai Wei, Minyou Chen , Senior Member, IEEE, Hongjian Xia, Dan Luo , Hanrui Li, Jinbao Zhang, and Hui Li , Member, IEEE

Abstract—Junction temperature is the most important factor to induce the insulated gate bipolar transistor module failure and conduct operational management. In-situ calibrated method and junction temperature calculation model are proposed to timely indicate the junction temperature for the electric vehicle drive system. It aims to solve that the conventional calibration methods need to be calibrated in the temperature chamber and the model cannot meet variable current conditions, which ignores the effects of the stray parameters of electrode connection on the on-state voltage. A mathematical junction temperature estimation model based on the relationship between saturation voltage drop and different currents is established, whose accuracy depends on the prior narrow range junction temperature calibration. A control strategy for the in-situ calibration is proposed to generate an instantaneous large current by creating a zero-torque condition and using integrated negative temperature coefficient thermistors, current sensor, and on-state voltage measured circuit when the new-energy vehicle is in an idle state. Experimental results prove that the proposed in-situ calibration method can be realized totally inside the electric vehicle, which can serve the full-service lifetime of the electric vehicle with high precision.

Index Terms—Insulated gate bipolar transistor (IGBT), junction temperature calibration, junction temperature estimation, negative temperature coefficient (NTC), reliability.

I. INTRODUCTION

REASONABLE development and utilization of new energy are important means to solve energy shortages and environmental pollution. As a key component of the electric vehicle, insulated gate bipolar transistor (IGBT) modules play the role

of energy transfer and power conversion. However, frequent start-stops, accelerations, and decelerations make IGBT withstand higher thermal stress fluctuations than in other application scenarios, which leads to a higher failure risk. According to the survey, it shows that 38% of ac system failures are caused by power device failure [1]. There are various failure modes for wire-bonded packaging power modules, the most commonly observed ones are packaging-related failures. The root cause of the predominant failure mechanisms, i.e., bond wire lift-off and solder delamination, is junction temperature cycling with the associated internal temperature gradient acting on the mismatch of coefficients of thermal expansion between adjacent layers and internal temperature gradients [2]. Therefore, to avoid operating failures of electric vehicles, it is necessary to obtain the IGBT junction temperature in the electric drive system using a real-time scheme.

Recently, many methods have been proposed, e.g., optical measurement method and physical contact method. However, these methods demand dismantling devices from converters and cannot meet the goal of online monitoring methods [3]. Thermal network models are used to acquire junction temperature based on the calculated power loss of devices, which heavily relies on the parameters of the thermal network and cannot ensure accuracy due to the aging effects of devices [4], [5], [6]. A thermal estimation method for the IGBT module is proposed, which is adaptable to operating conditions [7], however, the power loss needs to be calculated exactly. Sensor-based direct measurement is the second method using an infrared thermal camera or built-in thermal sensors on the silicon chip [8], however, the packing housing should be removed or changed.

Temperature-sensitive electrical parameters (TSEPs) use the terminal electrical parameters, which are easy to obtain and have a one-to-one relationship with the junction temperature of IGBTs for condition monitoring, such as small current injection method, turn-off time, turn-off delay time, etc. [9], [10], [11], [12], [13]. A converter-level IGBT junction temperature estimation method based on the dc bus voltage ringing is proposed, where an additional auxiliary heating unit is connected and used to calibrate the method [14]. There is a difference between the work condition and the calibration condition. An accurate junction temperature estimation method is proposed throughout its lifetime, which eliminates the effects of the bond-wire degradation [15], however, the updated I-V characteristics need

Manuscript received 14 April 2022; revised 4 July 2022; accepted 27 August 2022. Date of publication 6 September 2022; date of current version 10 October 2022. This work was supported in part by the National Natural Science Foundation of China-State Grid Corporation Joint Fund for Smart Grid under Grant U1966213, in part by the Fundamental Research Funds for the Central Universities under Grant 2022CDJKYJH009, in part by the Bidding Projects Announced by Shanxi Provincial Department of Science and Technology under Grant 20201101017, and in part by the National Key Research and Development Program of China under Grant 2018YFB0905800. Recommended for publication by Associate Editor J. Popovic-Gerber. (Corresponding author: Wei Lai.)

The authors are with the State Key Laboratory of Power Transmission Equipment and System Security and New Technology, School of Electrical Engineering, Chongqing University, Chongqing 400044, China (e-mail: laiwecqu@126.com; 956986267@qq.com; mchencqu@126.com; 912708187@qq.com; walluodan@163.com; 202011131068t@cqu.edu.cn; 202011131241@cqu.edu.cn; cqulh@163.com).

Color versions of one or more figures in this article are available at <https://doi.org/10.1109/TPEL.2022.3204547>.

Digital Object Identifier 10.1109/TPEL.2022.3204547

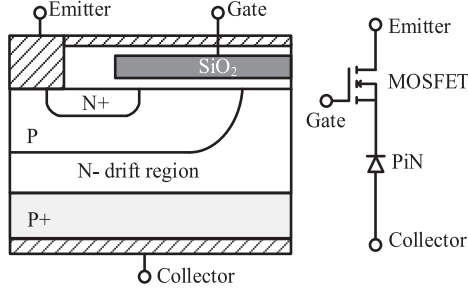


Fig. 1. Basic IGBT structure and equivalent on-state circuit.

to be measured offline. On-state collector-emitter voltage at higher collector currents is used to estimate the junction temperature, however, it only can be used for the constant current condition, which can meet the variable current conditions of the electric vehicles due to the polytropic speeds and motor torques [16]. Although TSEPs provide many possibilities for obtaining the junction temperature, almost all methods require calibration of the relationship between temperature-sensitive parameters and the junction temperature under laboratory conditions. Nevertheless, a small injection current source is connected in the circuit, and there are differences between the calibration environment and the actual working conditions. Meanwhile, the device status will degrade in service, which leads that the previous calibration parameters are no longer applicable.

There are two main contributions of this article: 1) A novel junction temperature estimated model based on the relationship between the junction temperature and the saturation voltage drop, which can be used for variable load current conditions, especially for the motor driver. 2) An repeatable in-situ calibration method is proposed to acquire the coefficients of the junction temperature estimation model with narrow temperature range under different degraded status, which gets rid of the limitation of the traditional junction temperature non-in-situ calibration that the devices need to be placed in a temperature chamber or be placed on an auxiliary heating unit. This scheme exploits the current sensor in the motor driver, the integrated negative temperature coefficient (NTC) in the module, and the low-cost on-state voltage measurement circuit to calibrate the corresponding coefficients in the model when the electric vehicle is idle. This junction temperature estimated model can be calibrated during the full-service cycle of electric vehicles. It can be used for high-precision real-time acquisition of the junction temperature to improve the operation reliability of electric vehicles.

II. ONLINE JUNCTION TEMPERATURE CALCULATION MODEL

A. Relationship Between On-State Voltage and Junction Temperature

According to the internal structure of IGBT chips and the simplified on-state circuit shown in Fig. 1, the on-state voltage V_{CE_ON} of the chip contains two parts as shown in (1) [17], where V_{PiN} is the internal equivalent diode conduction voltage

drop, and V_{MOSFET} is the internal equivalent MOSFET conduction voltage drop

$$V_{CE_ON} = V_{PiN} + V_{MOSFET} \quad (1)$$

V_{PiN} can be written in the form of the following equation:

$$V_{PiN} = \frac{2k \cdot T}{q} \ln \left[\frac{I_c \cdot W_N}{4q \cdot D_a \cdot n_i \cdot p \cdot Z \cdot F(W_N/2L_a)} \right] \quad (2)$$

where k is the Boltzmann coefficient, T is the thermodynamic temperature, q is the charge of an electron, I_c is the on-state current of the IGBT, D_a is the bipolar diffusion coefficient, n_i is the intrinsic carrier concentration, p is the chip cell size, Z is the cell width perpendicular to the direction of cross-section, W_N is the N-type base region width, L_a is the ambipolar diffusion length, d is the half-width of the drift region. The function $F(W_N/2L_a)$ can be expressed as (3) [17], where V_M is the conduction voltage drop in the drift region

$$F(W_N/2L_a) = \frac{\frac{W_N}{2L_a} \tanh \frac{W_N}{2L_a}}{\sqrt{1 - 0.25 \tanh^4 \left(\frac{W_N}{2L_a} \right)}} e^{-\frac{qV_M}{2kT}}. \quad (3)$$

When the MOSFET works in the linear zone, conduction voltage drop V_{MOSFET} can be expressed as [17]

$$V_{MOSFET} = \frac{I_c \cdot L_{CH}}{Z \cdot \mu_{ni} \cdot C_{OX} \cdot (V_G - V_{TH})} \quad (4)$$

where L_{CH} is the length of the channel, μ_{ni} is the electron migration rate, C_{OX} is the capacitance of the gate oxide layer, V_G is the gate drive voltage, and V_{TH} is the threshold voltage of the gate.

Hence, the on-state voltage of chip V_{CE_ON} can be rewritten as

$$V_{CE_ON} = \frac{2k \cdot T}{q} \ln \frac{I_c \cdot W_N}{4q \cdot D_a \cdot n_i \cdot p \cdot Z \cdot F(W_N/2L_a)} + \frac{I_c \cdot L_{CH}}{Z \cdot \mu_{ni} \cdot C_{OX} \cdot (V_G - V_{TH})}. \quad (5)$$

Since the thermal behavior of the materials is different under different temperatures, the temperature dependences of D_a , n_i , μ_{ni} , and V_{TH} are expressed as

$$D_a = \frac{1.5 \times 10^9 k \cdot T^{-1.33}}{q \cdot (1 + 5.52T^{-0.1})} \quad (6)$$

$$n_i = 3.87 \times 10^{16} T^{1.5} \cdot e^{-\frac{7020}{T}} \quad (7)$$

$$\mu_{ni} = 1360 \times \left(\frac{T}{300} \right)^{-2.42} \quad (8)$$

$$V_{TH} = \frac{\sqrt{4\varepsilon_{si}K \cdot T \cdot N_A \cdot \ln(N_A/n_i)}}{C_{OX}} + 2 \frac{K \cdot T}{q} \cdot \ln \left(\frac{N_A}{n_i} \right). \quad (9)$$

When the gate voltage is much higher than the threshold voltage, the internal equivalent MOSFET in the IGBT structure works in the linear region, and the internal equivalent MOSFET conduction resistance R_{DS_ON} at this time can be approximated

using (10), where R_0 is the initial resistance, T_j is the junction temperature, and m is the temperature coefficient

$$R_{DS_ON} = R_0 + m \cdot T_j. \quad (10)$$

Substituting (10) into (5), V_{CE_ON} can be rewritten as

$$V_{CE_ON} = \frac{2k \cdot T}{q} \ln \frac{I_c \cdot W_N}{4q \cdot D_a \cdot n_i \cdot p \cdot Z \cdot F(W_N/2L_a)} + I_c \cdot (R_0 + m \cdot T_j) \quad (11)$$

Substituting (3), (6) and (7) into (11), V_{CE_ON} can be rewritten and simplified further as (12), where k_1 is expressed as (13), and k_2 is expressed as (14)

$$V_{CE_ON} = k_1 \cdot T_j \cdot \left(\ln(k_2 \cdot I_c) - \ln \frac{T_j^{0.17}}{1 + 5.52T_j^{-0.1}} + \frac{7020}{T_j} + \frac{q \cdot Vm}{2K \cdot T_j} \right) + I_c \cdot (R_0 + m \cdot T_j) \quad (12)$$

$$k_1 = \frac{2k}{q} \quad (13)$$

$$k_2 = \frac{W_N \cdot \sqrt{1 - 0.25 \tanh^4 \left(\frac{W_N}{2L_a} \right)}}{6 \times 10^9 \times 3.87 \times 10^{16} k \cdot p \cdot Z \cdot \frac{W_N}{2L_a} \tanh \frac{W_N}{2L_a}}. \quad (14)$$

In actual applications, usually the junction temperature T_j is typically situated between 273 and 423 K. The range of (15) is $[-0.48, 0.36]$, and the range of $7020/T_j$ is [17], [25]. Therefore, (15) can be ignored by comparing with the $7020/T_j$, and V_{CE_ON} can be simplified as (16)

$$f(T_j) = \ln \frac{T_j^{0.17}}{1 + 5.52T_j^{-0.1}} \quad (15)$$

$$V_{CE_ON} \approx k_1 \cdot \left(T_j \cdot \ln(k_2 \cdot I_c) + 7020 + \frac{q \cdot Vm}{2K} \right) + I_c \cdot (R_0 + m \cdot T_j). \quad (16)$$

T_j can be rewritten as (17). Where $m_1 \sim m_5$ are related to IGBT structure and materials, and these parameters can be extracted using function fitting under different collector currents I_c

$$T_j \approx \frac{V_{CE_ON} - m_4 \cdot I_c - m_5}{m_1 \cdot \ln(m_2 \cdot I_c) + m_3 \cdot I_c}. \quad (17)$$

From the (17), when $m_1 \cdot \ln(m_2 \cdot I_c) + m_3 \cdot I_c \approx 0$, it means that T_j has no relationship with the V_{CE_ON} . This work condition is the zero temperature coefficient point as shown in Fig. 2 [18], which is the relationship between collector current and collector-emitter voltage of the INFINEON FF600R12ME4 IGBT module (1200 V/600 A) extracted from the datasheet, which is usually used for electric vehicles. When $m_1 \cdot \ln(m_2 \cdot I_c) + m_3 \cdot I_c > 0$, T_j is in proportion to V_{CE_ON} , which corresponds to the zone of the positive temperature coefficient. When $m_1 \cdot \ln(m_2 \cdot I_c) + m_3 \cdot I_c < 0$, T_j is inversely proportional to V_{CE_ON} , which corresponds to the zone of the NTC. The value ranges can be used as

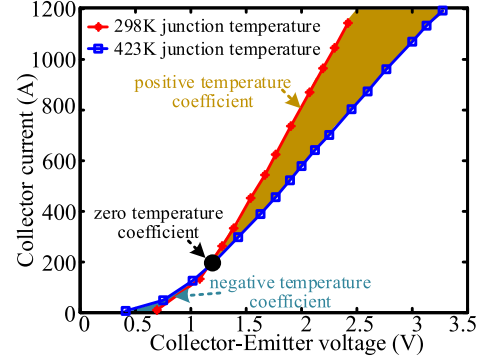


Fig. 2. Relationship between collector current and collector-emitter voltage.

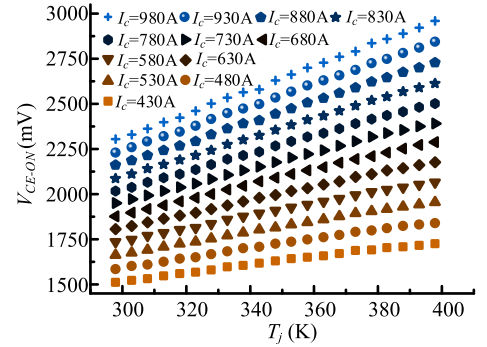


Fig. 3. Forward conduction characteristics of IGBT in 298–398 K [16].

the constraints to solve the parameters (17). It can be used to qualitatively prove that the derived model is reasonable.

B. Analysis of Temperature Calculation Model Characteristics

Experimental data are selected as an example for analysis in the literature [19]. The forward conduction characteristics of IGBT modules in the temperature range of 298–398 K are shown in Fig. 3. Those data are used to fit the coefficients of (17) and the traditional model, which uses a cubic polynomial model as shown in (18). Where $a, b, c, d, e, f,$ and g are obtained using the function fitting. The parameters $a, b, c, d, e, f,$ and g of the cubic polynomial model are $-412.8619, 0.9677, -0.6650, -0.001599, 0.002607, 7.8652E-7,$ and $-1.5955E-6,$ respectively. The parameters $m_1, m_2, m_3, m_4,$ and m_5 of the proposed model are $0.2392, 0.00003206, 0.007498, -0.9193,$ and $1255.7169,$ respectively. Fig. 4 shows the fitting errors of the two models. Pearson's correlation coefficient of determination R^2 is calculated to check the fitting strength, the correlation coefficient is $0.9979,$ and the sum of squares due to error (SSE) is $464.$ R^2 of the proposed model is $0.9985,$ and the SSE is $342.$ The results confirm that the above two models fitted with calibration data in the full temperature range can reflect the variation of junction temperature with on-state voltage and collector current well, however, the proposed model is more accurate

$$T_j = a + b \cdot V_{CE_ON} + c \cdot I_c + d \cdot I_c \cdot V_{CE_ON} + e \cdot I_c^2 + f \cdot I_c^2 \cdot V_{CE_ON} + g \cdot I_c^3. \quad (18)$$

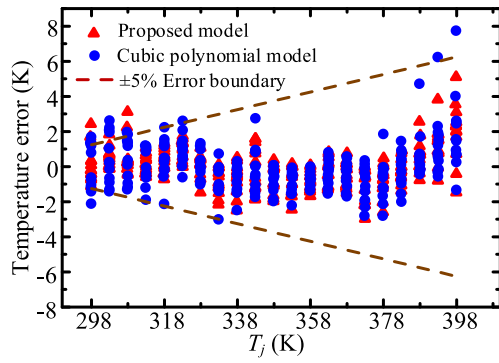
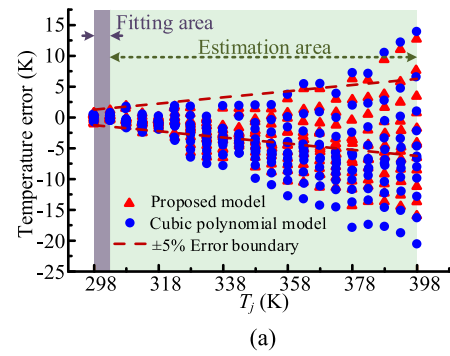


Fig. 4. Fitting errors of the two models in temperature.

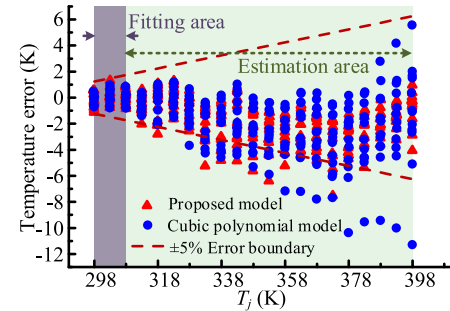
It can be seen that it is beneficial to calibrate the temperature-sensitive parameters of the IGBT modules over the full work condition temperature range. However, the calibration over the full temperature range requires taking the IGBT modules out of the system and placing them in the temperature chamber, which is inconvenient. It leads that there is a working condition difference with or without in-situ calibration, because stray parameters of electrode connection are not considered. If the temperature-sensitive parameter calibration can be performed in the actual system where the device is located, the influence of interconnection can be avoided for traditional methods to improve the junction temperature estimation accuracy. In addition, the calibration in the system will be free from the traditional and complex manual calibration process, and it can be calibrated multiple times in the system to overcome the changes in the temperature-sensitive parameter relationship caused by the aging of the devices.

One of the problems faced in achieving in-system calibration of the device is the lack of a wide range of temperature changes. Based on (17), the junction temperature has an approximately linear relationship with the on-state voltage of IGBT modules when the collector current is constant, and the function fitting of the linear relationship can be completed with a small amount of data. Therefore, the calibration data in the temperature range of 298–303 K, 298–308 K, 298–313 K, and 298–318 K are used to fit the (17) and (18) respectively, and the fitted models are used to predict the junction temperature of the IGBT modules in the high-temperature region. Fig. 5 shows the junction temperature prediction errors of the two models for the four temperature regions respectively. Fig. 6(a) compares the R^2 and SSE of the fitted models under different temperature regions.

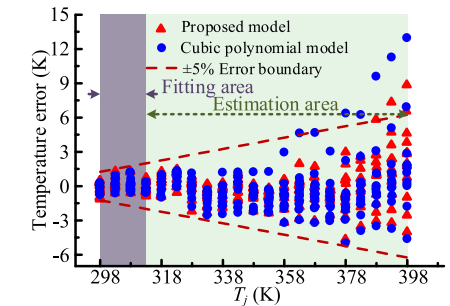
Fig. 5(a) shows that the models predict the junction temperature with a large error due to the extremely narrow temperature range. With the temperature range expansion of the fitted data, as shown in Fig. 5(b) and (c), it can be seen that the temperature range can improve the model accuracy sharply, and the overall prediction error can be limited to 5%. However, with the temperature range of the fitted data further expansion, the prediction accuracy of the models is improved slowly as shown in Fig. 5(d). From Figs. 5 and 6(a), it can be concluded that the proposed model has better extrapolation performance than



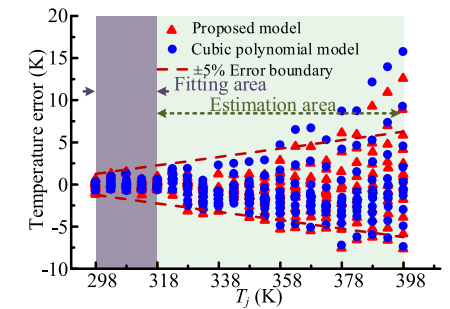
(a)



(b)



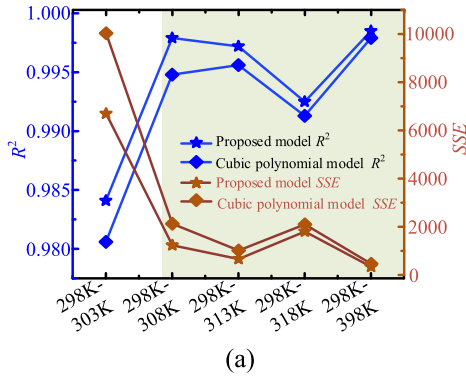
(c)



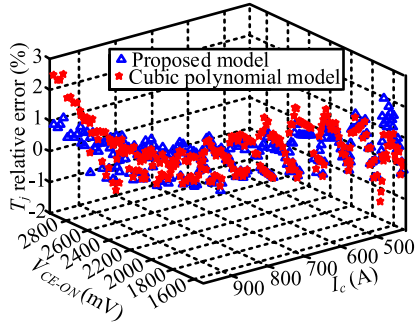
(d)

Fig. 5. Estimation error of the models fitted with different temperature regions. (a) 298–303 K. (b) 298–308 K. (c) 298–313 K. (d) 298–318 K.

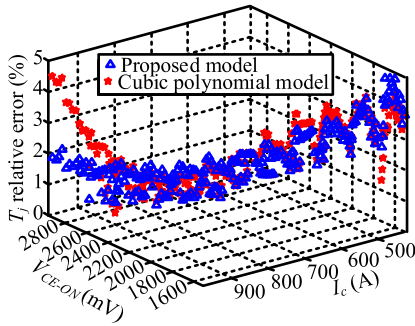
the cubic polynomial model under the same narrow temperature range. Fig. 6(a) shows that it can meet the calibration requirements when the junction temperature is from 298 to 308 K. Fig. 6(b) and (c) shows the T_j relative error with and without considering the measured error using the above narrow junction temperature range, where the assumed measured error is 3% for V_{CE_ON} and I_C . It can be seen that the cubic polynomial model has low accuracy considering the measured error, especially with high currents.



(a)



(b)



(c)

Fig. 6. Fitting results analysis. (a) Performance comparison of the two models fitted with different temperature regions. (b) T_j relative error without considering the measured error. (c) T_j relative error considering the measured error.

The proposed method relies on the forward conduction characteristic of IGBT modules with a good linear relationship between the junction temperature and on-state voltage when the current is constant. Substituting the currents from 430 to 980 A into (16), the linear relationship can be obtained as shown in Fig. 7. Therefore, it can use a series of straight lines to restore the characteristic.

The proposed model fitted through the full temperature range can represent the forward conduction characteristics of IGBT modules well. It means that the straight lines produced by the model at any current level can pass through the calibration data uniformly. However, using a narrow temperature range of the fitted data to calibrate the model will lead that the model does not have good junction temperature prediction accuracy in all temperature regions, because the straight-line slope and intercept fitted by the narrow temperature range deviate from

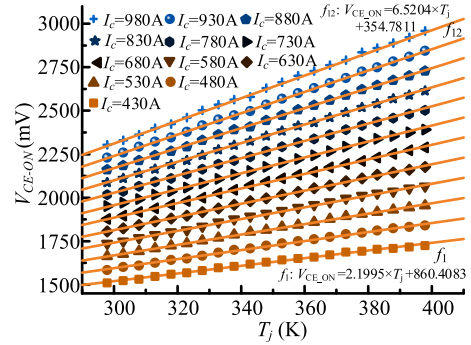


Fig. 7. Straight lines to restore the characteristic forward conduction of IGBT modules.

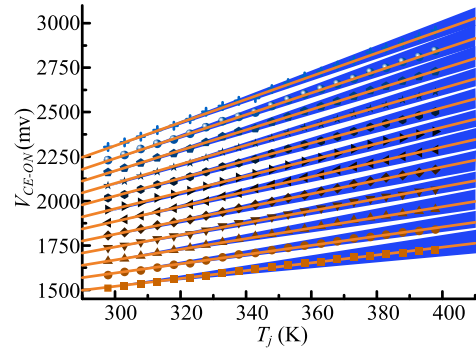


Fig. 8. Differences in the model fitted by different temperature zones.

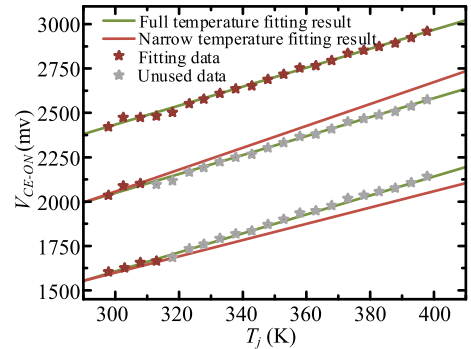


Fig. 9. Estimation error caused by the error of slope and intercept.

the model fitted by the full temperature range. The straight line fitted by the narrow temperature range may lie in the blue area, as shown in Fig. 8. Fig. 9 shows that the errors of the slope and intercept cause the prediction error in the IGBT junction temperature.

To more intuitively reflect the difference between the slopes and intercepts of the data fitting models in different temperature ranges for different current levels, the slopes and intercepts obtained by fitting the proposed model under different currents in the full temperature range are used as reference values. Fig. 10(a) compares the difference in slope between the reference and the fitted results with narrow temperature ranges for each constant current. As can be seen from Fig. 10(a), the slopes obtained

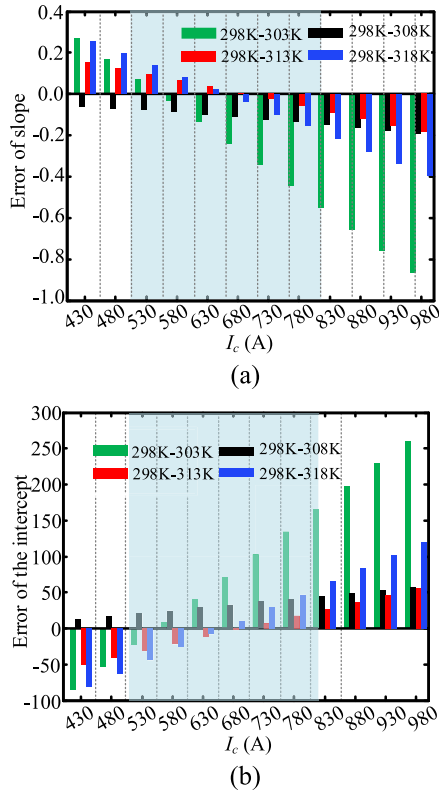


Fig. 10. Error of the model parameters. (a) Error of slope. (b) Error of intercept.

in the 298–308 K temperature range are all smaller than the reference slope, and the slopes of other temperature regions gradually change from greater than the reference slope to less than the reference slope with the increase of the current level. The middle section (shallow green) has a small slope error. The intercept also has a similar variation to the current level, and there is a small error around the middle current level, as shown in Fig. 10(b). Combing Figs. 5, 10, and 11, it can be seen that the estimated junction temperature error is caused by the slope and intercept difference. Note that the fitting narrow temperature range is selected according to the estimated error of the proposed model.

Comparing the differences in the slope and intercept with the reference value, the current and temperature ranges determine the prediction accuracy of the junction temperature. Therefore, the junction temperature calculation model fitted by the narrow temperature range calibration data has a relatively higher accuracy around medium current levels. For better performance, the working current level of the IGBT modules should be located in the middle of the calibration current level as much as possible according to Fig. 11.

III. CALIBRATION STEPS INSIDE THE ELECTRIC VEHICLE

To determine the coefficients in (17), many groups of data regarding T_j , I_c , and V_{CE_ON} need to be obtained. Different from the conventional calibration method, this article proposes that the calibration process can be accomplished using the information offered by the NTC thermistors welded inside the IGBTs

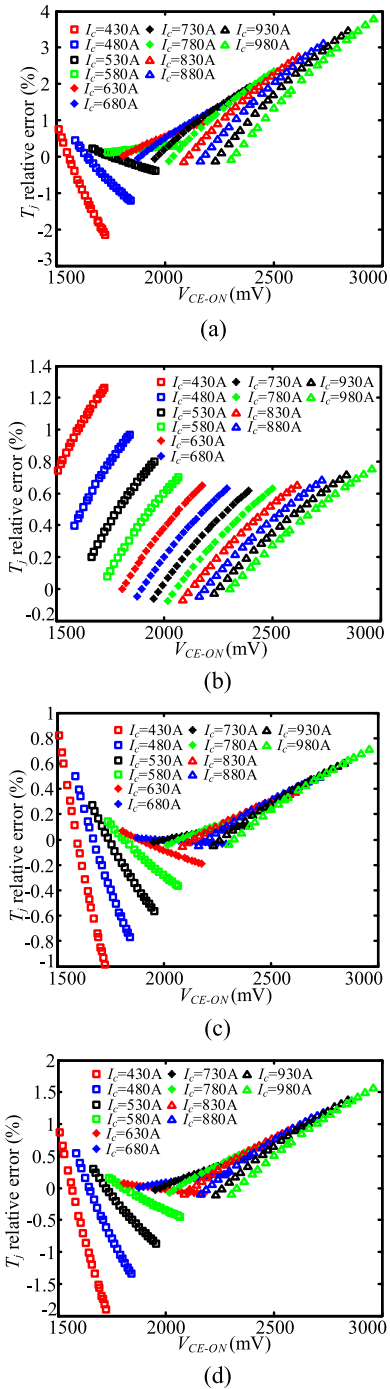


Fig. 11. Relative error of the junction temperature with different temperature regions. (a) 298–303 K. (b) 298–308 K. (c) 298–313 K. (d) 298–318 K.

when the new-energy vehicle is in an idle state. The control of the in-situ junction temperature calibration is described below.

A. Junction Temperature Measurement With an NTC Thermistor

In high-power IGBT modules, thermistors with NTCs are directly welded on the ceramic layer [20], [21]. The temperature of the ceramic layer can easily be obtained using the thermistors, as shown in Fig. 12(a). According to the thermal path, an

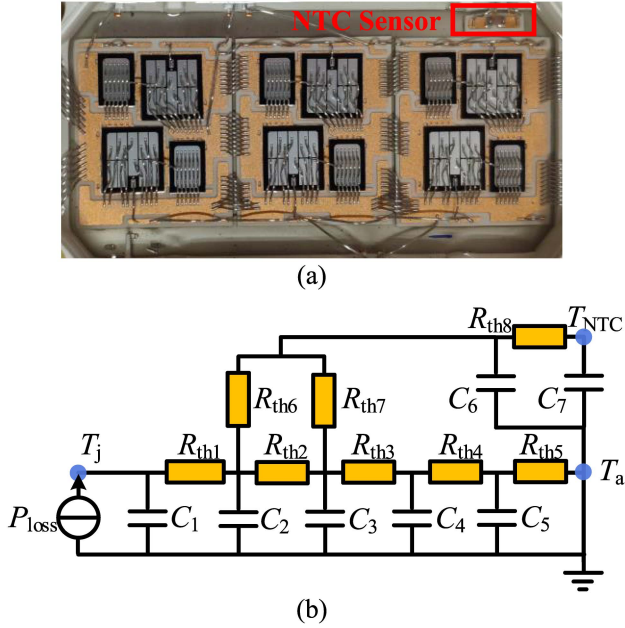


Fig. 12. IGBT structure with NTC sensor. (a) IGBT module with NTC. (b) Thermal network.

equivalent junction-to-NTC Cauer network of IGBT modules can be represented, as shown in Fig. 12(b), where P_{loss} indicates the power loss of the silicon chip, R_{thx} and C_x refer to the thermal resistance and capacitance of different layers, T_{NTC} is the temperature measured by the NTC sensor. However, it is too complicated to obtain the parameters. NTC is usually used for protection purposes, that is, when the temperature inside the module exceeds a certain value, the converter is considered to be in a dangerous condition or malfunctioning. When $P_{loss} \approx 0$ and the modules do not work for some time, it can be seen that T_j is approximately equal to T_{NTC} . Therefore, the electric vehicle is not used, and the measured temperature of the NTC is equal to the junction temperature of the IGBT modules, which is close to the ambient temperature. The temperature of the NTC can be obtained by (19), where R_{NTC} is the resistance of the NTC thermistors at the current temperature, B is the material constant of the NTC thermistors and R_{298} is the resistance of the NTC at 298 K. In order to calculate the temperature of the NTC, the value B needs to be used. Since the temperature is the module temperature when the electric vehicle is idle, the B value is selected as $B_{298/323}$ for higher precision

$$T_{NTC} = \frac{1}{\ln\left(\frac{R_{NTC}}{R_{298}}\right) / B + \frac{1}{298}}. \quad (19)$$

B. Generation of Large Current at Stationary State

When the new-energy vehicle is in an idle state, the calibration can be conducted, and the control of in-situ junction temperature calibration is shown in Fig. 13. There are two-time phases in a sequence, as described below: 1) Predetermined location stage: in the calibration stage, a sudden pulse signal of the torque might

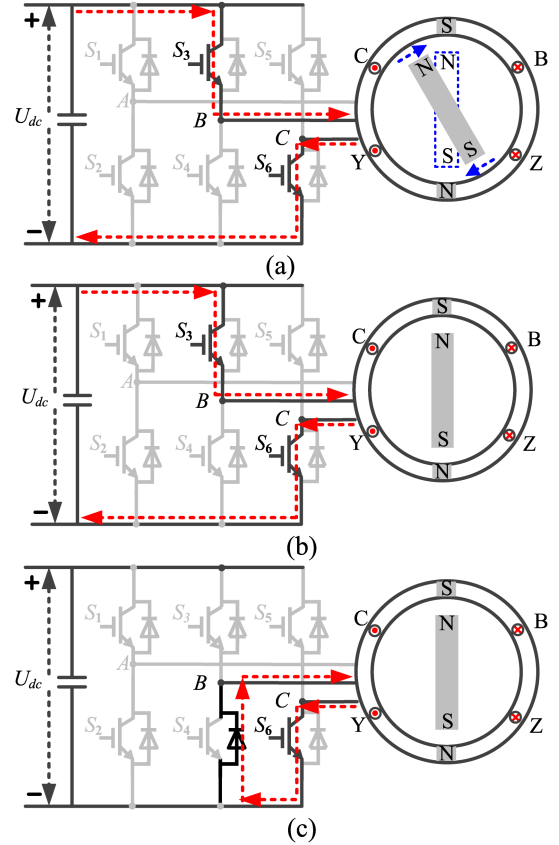
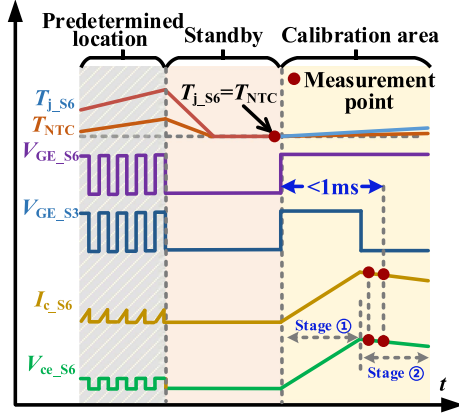


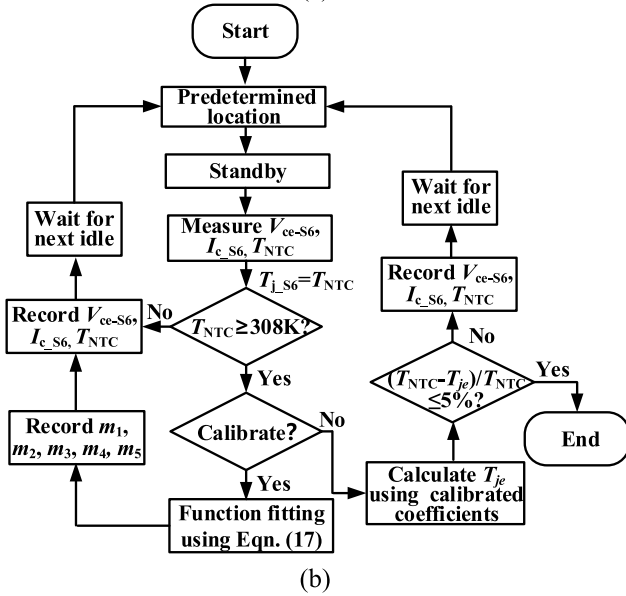
Fig. 13. Block diagram of the proposed junction temperature calibration. (a) Predetermined location stage. (b) Stage ① for calibration. (c) Stage ② for calibration.

cause the potential risk, and the predetermined location control method of the rotor should be proposed to avoid the risk. The calibration of the lower bridge arm IGBT module for phase C is taken as an example, and the schematic diagram is shown in Fig. 13(a). Where $S_1, S_2, S_3, S_4, S_5,$ and S_6 are IGBT modules for phases A, B, and C, respectively. The rotor initial position of the idle electric vehicle is assumed as shown in Fig. 13. The gate signals of S_3 and S_6 are set as the chopped wave as shown in Fig. 14, and the rest switches are turned OFF, which will generate a stator current. A magnetic field is formed under this current, and the rotor will be rotated to the position of the blue dotted line rectangle.

2) Calibration stage: a short-time high-level voltage signal for S_3 , the switch S_6 is always turned ON, and the rest switches are turned OFF as shown in Fig. 13(b). A large current is generated under zero torque conditions to reach the on-state voltage of the IGBT modules' work zone, which is usually designed from 0.9 to 1.1 times the working current, and the electric vehicle will not move as shown in Fig. 14(a) stage ①. V_{CE_ON} , NTC temperature T_{NTC} and I_c are measured at the same time with instantaneous reduced current values as shown in Fig. 14(a) stage ② and Fig. 13(c). In this condition, the power loss could be considered as nearly zero at this time, and the NTC temperature is equal to the junction temperature. The calibration flowchart is



(a)



(b)

Fig. 14. Calibration stage. (a) T_{NTC} , V_{CE_ON} , and I_c measurement sequence considering transient oscillation. (b) Calibration flowchart.

shown in Fig. 14(b), where the T_{je} is the estimated junction temperature using calibrated coefficients. The calibration flowchart can be divided into three parts. The first part is the preparatory and data acquisition stage. The second part is the function fitting stage using (17), where the calibrated temperature range is designed from 298 to 308 K. The third part is the verification stage.

C. Measurement Method of V_{CE_ON}

To measure V_{CE_ON} in the proposed calibration process and monitor the junction temperature, a special V_{CE_ON} measurement circuit that has the advantages of large voltage blocking capability and high-precision measurement is utilized [22], [23]. Collector-emitter voltage of IGBT modules will withstand dc bus voltage (hundreds of volts) during turn-OFF time, and it drops to a few volts when the modules turn ON. If V_{CE_ON} is measured directly, wide-range measurements will inevitably affect the measurement accuracy. Moreover, IGBT modules work at a

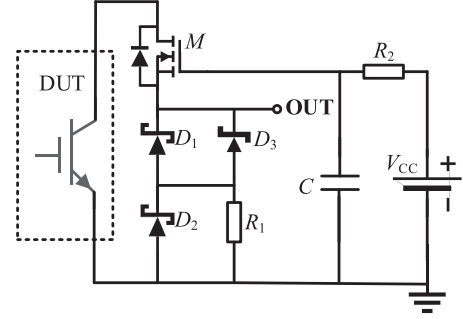


Fig. 15. On-state voltage measurement circuit.

TABLE I
TEST PLATFORM PARAMETERS

parameter	value
Motor model	TY-132M1
Busbar voltage	300V
Motor power	7.5kW
Pole pairs	3
Direct axis inductance	3.69mH
Quadrature axis inductance	9.39mH
Stator resistance	0.44 Ω
Flux linkage	0.4wb
Switching frequency	10kHz
IGBT type	FP10R12W1T4

higher switching frequency, and the measurement circuit needs to be able to respond quickly. Sensitivity for the junction temperature estimation is about 1–10 mV/ $^{\circ}\text{C}$. Therefore, it is hoped that the measurement accuracy of the V_{CE_ON} measurement circuit is as high as ± 1 mV. To meet the above-mentioned requirements, a special V_{CE_ON} measurement circuit can be used as shown in Fig. 15 [24], which has a simple topology and only needs a small hardware cost to realize the online measurement of V_{CE_ON} in an electric drive system, where $D_1 = D_2 = \text{IN4148}$, $D_3 = \text{1N4733}$, $R_1 = 10 \Omega$, $R_2 = 20 \Omega$, $C = 10 \text{ nF}$, and $M = \text{IRFR310}$. It is worth noting that the IGBT may experience a transient oscillation due to the influence of parasitic parameters during the turn-ON period. Therefore, V_{CE_ON} measurement should be carried out when the IGBT reaches a steady-state to improve the measurement accuracy, which is shown in Fig. 14(a).

IV. EXPERIMENT VALIDATION

To validate the effectiveness and precision of the proposed calibration schemes under a locked-rotor condition, a test bench is established, where the IGBT current is dc. Due to the laboratory equipment limitation, the high-power electric vehicle drive system (Changan SL03 auto 160kW/354V) is simplified into a small-power motor pair drag test platform (300 V/7.5 kW), where the motor's rating current is 11 A and the monitored IGBT module is selected as FP10R12W1T4 correspondingly. Table I shows the parameters. A K-type thermal couple is mounted on the Si chip to measure the junction temperature to validate the

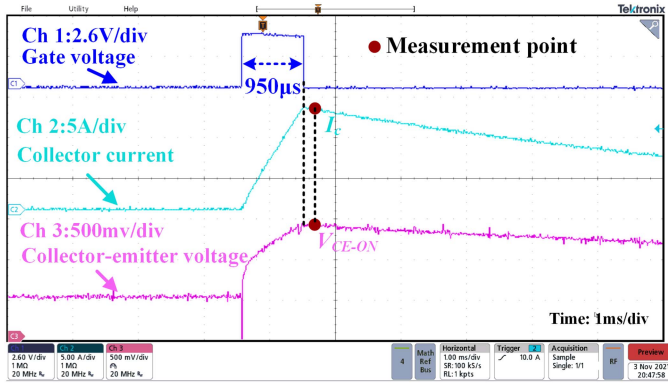
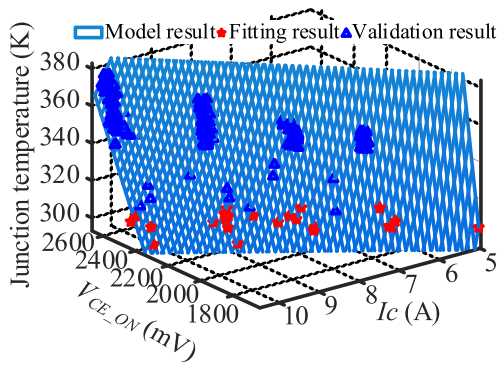
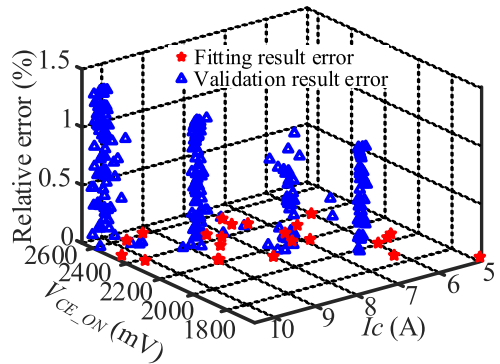


Fig. 16. Tested results for calibration schemes.



(a)

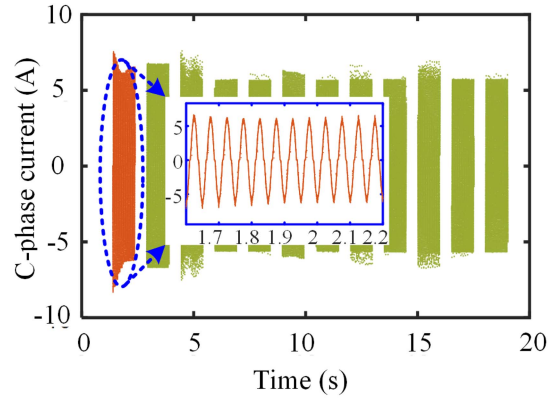


(b)

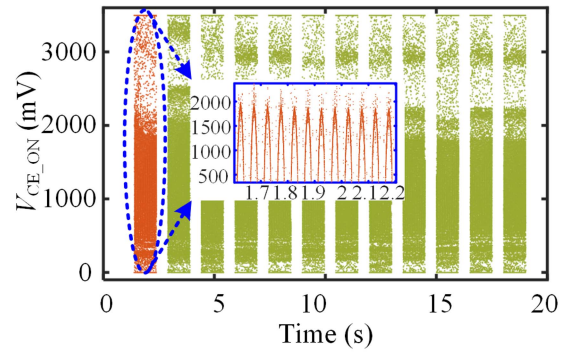
Fig. 17. Function fitting results and relative error for the dc condition. (a) Function fitting results. (b) Relative error.

junction temperature calculation method. NI-9214 acquisition card is adapted to process the information of thermocouples with 68S/s maximum sampling rate and $\pm 0.37^\circ\text{C}$ measurement accuracy. CYBERTEK-CP8300A current clamp with $\pm 10\text{ mA}$ accuracy is used to collect the current, and the data is processed by NI USB-6356, whose sampling rates can reach 1.25 MS/s with $\pm 1.4\text{ mV}$ sampling accuracy. The measured results for one single sample period are shown in Fig. 16, where the blue curve is the gate voltage (Ch 1), the laurel-green curve is the collector current (Ch 2), and the pink curve is the V_{CE_ON} (Ch 3).

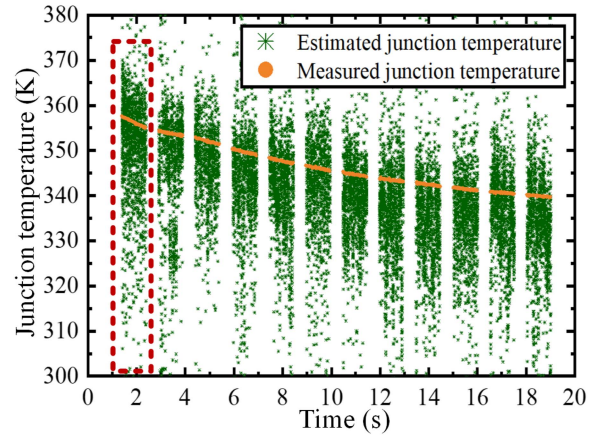
IGBTs are tested in the motor pair drag test platform with an ambient temperature ranging from 297 to 314 K. The calibrated



(a)



(b)



(c)

Fig. 18. Model and experiment results for the application condition. (a) C-phase current. (b) V_{CE_ON} result. (c) Experimental and measured junction temperature.

collector current range is set as 5–11 A because the peak value of the current is 6–10 A during normal operation. Function fitting is used to obtain the model parameters as shown in Fig. 17. Model parameters $m_1, m_2, m_3, m_4,$ and m_5 are fitted to be 0.227217, 0.000437, 0.526972, -26.8406, and 1388.148, respectively. Pearson's correlation coefficient is calculated to check the function fitting robustness and the correlation coefficient is 0.9876, which implies a strong correlation. Fig. 17(a) shows that a narrow range junction temperature from 297 to 314 K (red five-star marker) is used to obtain the parameters of (17), and it can be applied to other conditions (blue triangle marker). Good agreement is

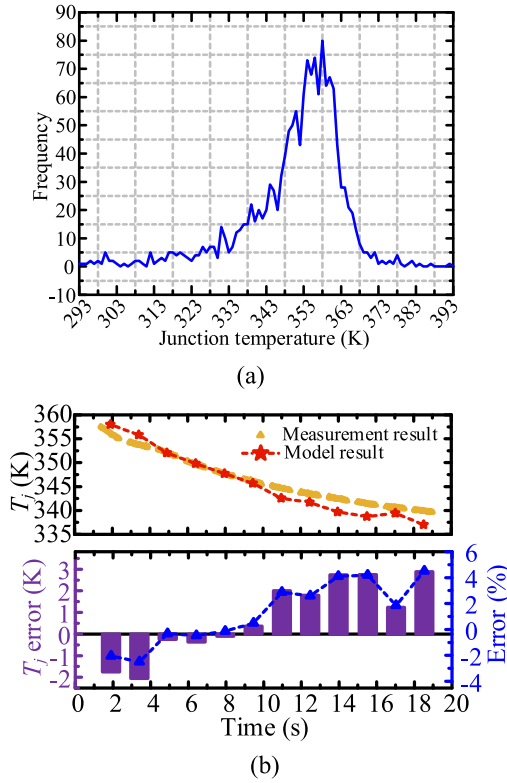


Fig. 19. Model and experiment results for the application condition. (a) Statistics results of frequency. (b) Junction temperature results.

observed, and the relative error is less than 2% as shown in Fig. 17(b), confirming that the model can be confidently used for calculating T_j .

To further demonstrate the feasibility and effectiveness of the model, an application condition is designed as shown in Fig. 18(a). On-state voltage V_{CE_ON} is measured using the circuit as shown in Fig. 15, and the results are shown in Fig. 18(b). 18(b) shows that some noise is inevitably collected, and it causes the estimated junction temperature to deviate from the real junction temperature as shown in Fig. 18(c). However, the overall predicted junction temperatures are densely distributed on both sides of the real values. An appropriate filtering algorithm is used to obtain more accurate estimated values. The filter algorithm counts the number of occurrences $F(T_{jei})$ of each calculated junction temperature T_{jei} in one second, which is calculated using (17), and $F(T_{jei})$ are listed in descending order as shown in the following equation:

$$F(T_{je1}) \geq F(T_{je2}) \geq \dots \geq F(T_{jen}). \quad (20)$$

The estimated junction temperature T_{jest} can be obtained using (21), where the M is the threshold value and it is set as 2 in this article

$$T_{jest} = \frac{\sum_{i=1}^M F(T_{jei}) \cdot T_{jei}}{\sum_{i=1}^M F(T_{jei})}. \quad (21)$$

The statistical results for Fig. 18(c) red dotted box are shown in Fig. 19(a). The highest frequency is extracted from the

statistical results as the weighted average, and a filter based on the temperature frequency distribution is designed to deal with the estimated junction temperature. After filter processing, estimated and measured junction temperatures are shown in Fig. 19(b). Comparing the calculated junction temperature with the measured results, it can be seen that the filtered junction temperature is similar to the junction temperature measured by the thermocouple, and the largest error is less than 5%. Therefore, the proposed junction temperature calculated model could be suitably used to support active junction temperature control, condition monitoring, and lifetime estimation in operational management.

V. CONCLUSION

In this article, an in-situ calibrated junction temperature calculation method is proposed to timely obtain the junction temperature under different conditions, when the new-energy vehicle is in an idle state. This article deduces the simplified mathematical relationship between junction temperature, collector current, and on-state voltage according to the physical structure of IGBT modules, whose parameters can be solved by experimental calibrations. Based on the linear relationship between the on-state voltage and the junction temperature at high currents, it is proposed to use a narrow range junction temperature to extract the parameters of the calculation method, and it can be then extrapolated to the other operation condition. A control strategy for the in-situ calibration is proposed to generate the calibrated operating condition, and a filtering algorithm based on the temperature frequency distribution is designed to reduce the measurement noise. The effectiveness of the junction temperature estimation model for the electric drive system is validated experimentally, and the largest error is less than 5%. This work can be usefully fed into the development of condition monitoring and lifetime estimation.

REFERENCES

- [1] F. W. Fuchs, "Some diagnosis methods for voltage source inverters in variable speed drives with induction machines - A survey[C]," in *Proc. IECON'03 29th Annu. Conf. IEEE Ind. Electron. Soc. (IEEE Cat. No.03CH37468)*, 2003, vol. 2, pp. 1378–1385.
- [2] K. Desingu, R. Selvaraj, and T. R. Chelliah, "Control of reactive power for stabilized junction temperature in power electronic devices serving to a 250-MW asynchronous hydrogenerating unit," *IEEE Trans. Ind. Appl.*, vol. 55, no. 6, pp. 7854–7867, Nov./Dec. 2019.
- [3] Y. Zhu, M. Xiao, X. Su, K. Lu, Z. Wu, and G. Yang, "IGBT junction temperature measurement under active-short-circuit and locked-rotor modes in new energy vehicles," *IEEE Access*, vol. 8, pp. 114401–114412, 2020.
- [4] Y. Yang, Q. Zhang, and P. Zhang, "A fast IGBT junction temperature estimation approach based on ON-state voltage drop," *IEEE Trans. Ind. Appl.*, vol. 57, no. 1, pp. 685–693, Jan./Feb. 2021.
- [5] M. Xu, K. Ma, B. Liu, and X. Cai, "Modeling and correlation of two thermal paths in frequency-domain thermal impedance model of power module," *IEEE J. Emerg. Sel. Topics Power Electron.*, vol. 9, no. 4, pp. 3971–3981, Aug. 2021.
- [6] C. Wang, C. Tian, H. Cheng, and J. Deng, "A PWM method of H-Bridge converter with temperature rise balancing and minimization based on periodically alternating employment of power devices," *IEEE Trans. Power Electron.*, vol. 37, no. 9, pp. 11135–11151, Sep. 2022.
- [7] W. Guo et al., "A thermal estimation method for IGBT module adaptable to operating conditions," *IEEE Trans. Power Electron.*, vol. 36, no. 6, pp. 6147–6152, Jun. 2021.

- [8] H. Ren et al., "Quasi-distributed temperature detection of press pack IGBT power module using FBG sensing," *IEEE J. Emerg. Sel. Topics Power Electron.*, to be published, doi: [10.1109/JESTPE.2021.3109395](https://doi.org/10.1109/JESTPE.2021.3109395).
- [9] J. Chen, E. Deng, Y. Zhang, and Y. Huang, "Junction-to-case thermal resistance measurement and analysis of press-pack IGBTs under double-side cooling condition," *IEEE Trans. Power Electron.*, vol. 37, no. 7, pp. 8543–8553, Jul. 2022.
- [10] J. Zhang, M. Du, L. Jing, K. Wei, and W. G. Hurley, "IGBT junction temperature measurements: Inclusive of dynamic thermal parameters," *IEEE Trans. Device Mater. Rel.*, vol. 19, no. 2, pp. 333–340, Jun. 2019.
- [11] D. Xiang et al., "Noncontact monitoring of IGBT turn-OFF time using PWM switching ringing for inverter-fed machine systems," *IEEE Trans. Power Electron.*, vol. 36, no. 10, pp. 11055–11067, Oct. 2021.
- [12] M. Du, Y. Tang, M. Gao, Z. Ouyang, K. Wei, and W. G. Hurley, "Online estimation of the junction temperature based on the gate pre-threshold voltage in high-power IGBT modules," *IEEE Trans. Device Mater. Rel.*, vol. 19, no. 3, pp. 501–508, Sep. 2019.
- [13] H. Luo, Y. Chen, P. Sun, W. Li, and X. He, "Junction temperature extraction approach with turn-off delay time for high-voltage high-power IGBT modules," *IEEE Trans. Power Electron.*, vol. 31, no. 7, pp. 5122–5132, Jul. 2016.
- [14] Y. Yang and P. Zhang, "A novel converter-level IGBT junction temperature estimation method based on the bus voltage ringing," *IEEE Trans. Power Electron.*, vol. 37, no. 4, pp. 4553–4563, Apr. 2022.
- [15] A. Arya, A. Chanekar, P. Deshmukh, A. Verma, and S. Anand, "Accurate online junction temperature estimation of IGBT using inflection point based updated I–V characteristics," *IEEE Trans. Power Electron.*, vol. 36, no. 9, pp. 9826–9836, Sep. 2021.
- [16] H. Huang and P. A. Mawby, "A lifetime estimation technique for voltage source inverters," *IEEE Trans. Power Electron.*, vol. 28, no. 8, pp. 4113–4119, Aug. 2013.
- [17] B. J. Baliga, *Fundamentals of Power Semiconductor Devices*. Han Zhengsheng et al., Eds. Beijing, China: Publishing House of Electronics Industry, 2013, (in Chinese).
- [18] U.-M. Choi, F. Blaabjerg, S. Jørgensen, S. Munk-Nielsen, and B. Rannestad, "Reliability improvement of power converters by means of condition monitoring of IGBT modules," *IEEE Trans. Power Electron.*, vol. 32, no. 10, pp. 7990–7997, Oct. 2017.
- [19] P. Ghimire, K. B. Pedersen, I. Trintis, B. Rannestad, and S. Munk-Nielsen, "Online chip temperature monitoring using *v*_{ce}-load current and IR thermography," in *Proc. IEEE Energy Convers. Congr. Expo.*, 2015, pp. 6602–6609.
- [20] P. Liu, C. Chen, X. Zhang, and S. Huang, "Online junction temperature estimation method for SiC modules with built-in NTC sensor," *CPSS Trans. Power Electron. Appl.*, vol. 4, no. 1, pp. 94–99, Mar. 2019.
- [21] M. Ma et al., "Online junction temperature estimation using integrated NTC thermistor in IGBT modules for PMSM drives," *Microelectronics Rel.*, vol. 114, no. 12, 2020, Art. no. 113836.
- [22] F. Yang, C. Xu, and B. Akin, "Experimental evaluation and analysis of switching transient's effect on dynamic on-Resistance in GaN HEMTs," *IEEE Trans. Power Electron.*, vol. 34, no. 10, pp. 10121–10135, Oct. 2019.
- [23] R. Hou, Y. Shen, H. Zhao, H. Hu, J. Lu, and T. Long, "Power loss characterization and modeling for GaN-based hard-switching half-bridges considering dynamic on-state resistance," *IEEE Trans. Transp. Electrific.*, vol. 6, no. 2, pp. 540–553, Jun. 2020.
- [24] J. Würfl et al., "Dynamic drift effects in GaN power transistors: Correlation to device technology and mission profile," in *Proc. Int. Power Electron. Conf. (Niiigata ECCE Asia)*, 2018, pp. 3607–3612.



Wei Lai (Member, IEEE) received the M.Sc. degree from the Chongqing University of Technology, Chongqing, China, in 2012, and the joint Ph.D. degree from the University of Warwick, Coventry, U.K., in 2015, funded by the China Scholarship Council.

He is currently an Associate Professor in electrical engineering with the School of Electrical Engineering, Chongqing University, Chongqing, China. His current research interests include the reliability of power modules, the application of power electronics for electric power generation, and the development of

condition monitoring methods for power electronic converters.



Yunhai Wei received the B.Sc. degree from the Chongqing University of Technology, Chongqing, China, in 2019. He is currently working toward the M.Sc. degree in electrical engineering from Chongqing University, Chongqing, China.

His current research interests include condition monitoring, thermal management, and prediction techniques for real-time applications of power electronic devices.



Minyou Chen (Senior Member, IEEE) received the M.Sc. degree in control theory and engineering from Chongqing University, Chongqing, China, in 1987, and the Ph.D. degree in control engineering from the University of Sheffield, Sheffield, U.K., in 1998.

He is currently a Full Professor with Chongqing University. He has authored or coauthored more than 180 papers. His research interests include intelligent modeling and control, reliability of power modules, micro-grid control, and state monitoring in power distribution systems.



Hongjian Xia received the B.Sc. degree in college of instrument and electrical engineering from Jilin University, Changchun, China, in 2018. He is currently working toward the Ph.D. degree in electrical engineering with Chongqing University, Chongqing, China.

From 2021 to 2022, he was a Visiting Ph.D. Student with the AAU energy, Aalborg University, Aalborg, Denmark. His research interests include the reliability and control of modular multilevel converters and motor drives.



Dan Luo received the M.S. degree from the School of Electrical Engineering, Guizhou University, Guizhou, China, in 2016. He is currently working toward the Ph.D. degree in electrical engineering with the School of Electrical Engineering, Chongqing University, Chongqing, China.

His research interests include the reliability of power modules.



Hanrui Li received the B.Sc. degree from the Harbin University of Science and Technology, Harbin, China, in 2012. He is currently working toward the M.Sc. degree in electrical engineering with the School of Electrical Engineering, Chongqing University, Chongqing, China.

His research interests include the reliability of power modules.



Jinbao Zhang received the B.Sc. degree from the Sichuan Agricultural University, Yaan, China, in 2020. He is currently working toward the M.Sc. degree in electrical engineering with the School of Electrical Engineering, Chongqing University, Chongqing, China.

His research interests include the reliability of power electronic devices.



Hui Li (Member, IEEE) received the M.Eng. and Ph.D. degrees in electrical engineering from Chongqing University, Chongqing, China, in 2000 and 2004, respectively.

He was a Postdoctoral Research Fellow with the Institute of Energy Technology, Aalborg University, Aalborg, Denmark, from 2005 to 2007. Since 2008, he has been a Professor with the Department of Electrical Machinery and Electrical Apparatus, School of Electrical Engineering, Chongqing University. His main research interests include wind power generation,

design, and control of electrical machines.